Communications in Physics, Vol. 33, No. 3 (2023), pp. 235-250
DOI: https://doi.org/10.15625/0868-3166/18082

One-loop formulas for off-shell decay $H^* \to W^+W^-$ in 't Hooft-Veltman gauge and its applications

Khiem Hong Phan[1,2], **Dzung Tri Tran**[1,2] **and Anh Thu Nguyen**[3]

[1] *Institute of Fundamental and Applied Sciences, Duy Tan University, Ho Chi Minh City* 700000*, Vietnam*

[2] *Faculty of Natural Sciences, Duy Tan University, Da Nang City* 550000*, Vietnam*

[3] *University of Science Ho Chi Minh City,*
227 *Nguyen Van Cu, District* 5*, Ho Chi Minh City, Vietnam*

E-mail: †phanhongkhiem@duytan.edu.vn

Received 14 February 2023
Accepted for publication 23 May 2023
Published 7 August 2023

Abstract. *We present analytic results for one-loop radiative corrections to off-shell decay $H^* \to W^+W^-$ in 't Hooft-Veltman gauge within the Standard Model framework. In numerical results, we show off-shell decay rate and its corrections with varying off-shell Higgs mass. The results show that the corrections are of* 10% *contributions to the total decay rates. Furthermore, we study the impacts of one-loop radiative corrections to the off-shell decay $H^* \to W^+W^-$ in Higgs processes at future colliders. The signal processes such as $e^-e^+ \to ZH^* \to Z(WW)$ with including the initial beam polarizations and $e^-e^+ \to \nu_e\bar{\nu}_e H^* \to \nu_e\bar{\nu}_e(WW)$ and $e^-\gamma \to e^-H^* \to e^-WW$ are examined. We find that the effects are visible impacts and these should be taken into account at future colliders.*

Keywords: one-loop corrections; analytic methods for Quantum Field Theory; dimensional regularization; Higgs phenomenology.
Classification numbers: 03.70.+k; 11.10.-z.

1. Introduction

One of the main targets of future colliders like the high-Luminosity Large Hadron Collider (HL-LHC) [1, 2] and future colliders [3] is to measure accurately the properties of standard-model-like Higgs boson. From the experimental data, we can verify the nature of the scalar Higgs potential and understand deeply the electroweak spontaneous symmetry breaking. It means that all Higgs productions and decay channels should be probed precisely as possible. Among Higgs decay processes, off-shell Higgs decay to W-boson pair are considerable interest at present and future colliders [4–13]. Since the decay processes could provide an important information for understanding the Higgs sectors at higher-energy scales which are sensitive with new physics contributions.

Full one-loop electroweak corrections to Higgs decay to W-pair have been calculated in [14] and to $H \to W^*W^* \to 4$ leptons have performed in [15–18]. The calculations for one-loop radiative corrections to $H \to W^*W^* \to 4$ leptons in many of extensions for the SM have been reported in [19–22]. Due to the importance of the decay channel, we perform the calculations for one-loop radiative corrections to $H \to WW$ with the following extensions. We first provide analytic results for one-loop radiative corrections to $H \to WW$ for both off-shell Higgs and W-pair. As a result, our results are valid for one-loop correction to the vertex HWW which can be taken into account in many relevant process calculations. Moreover, we can apply double-pole approximation for studying off-shell Higgs decay to W-pair from the analytical results in this paper. In further, the study for the impacts of one-loop corrections to off-shell decay to W-pair through Higgs signal processes at future colliders like e^-e^+ collisions, photon-electron collisions. In the detail, our computations are performed in the 't Hooft-Veltman gauge in the framework of the SM. One-loop form factors for the off-shell decay are expressed in terms of scalar one-loop Passarino-Veltman functions in the standard notations of `LoopTools`. As a result, off-shell decay rates can be evaluated numerically by using this program. In phenomenological results, we show decay rates and the corrections as a function of off-shell Higgs mass. The results show that the corrections are of 10% contributions. In addition, we study the impacts of one-loop corrections to off-shell decay $H^* \to W^+W^-$ in Higgs processes at future colliders. Specially, all signal processes such as $e^-e^+ \to ZH^* \to Z(WW)$, $e^-e^+ \to f\bar{f}H^* \to f\bar{f}(WW)$ for $f = e, \nu_e$ and $e^-\gamma \to e^-H^* \to e^-WW$ are examined. In this analysis, we include the initial beam polarization effects and consider both the unpolarized case and the case of longitudinal polarizations for W bosons. We find that the effects are visible impacts and these must be taken into account at future lepton colliders.

The layout of the paper is as follows: In section 2, we first present one-loop expressions for the vertex HWW. We then apply these formulas to the off-shell Higgs decay channel $H^* \to WW$. We also take into account for soft and hard photon contributions in this section. In section 3, phenomenological results are shown. The impacts of one-loop off-shell Higgs decay through Higgs productions at future colliders are discussed in this section. Conclusions and outlook for this research are discussed in the section 4. In the appendix, we show the one-loop counter-term for HWW vertex. One-loop Feynman diagrams in the 't Hooft-Veltman gauge for this decay channel are shown in the appendix C.

2. Calculations

We present in detail the calculations in this section. All one-loop Feynman diagrams contributing to the vertex HW^+W^- in the 't Hooft-Veltman gauge can be classified into two groups (shown in appendix C). First, we consider all fermions propagating in the loop diagrams to group 1 (called as G_1). In the group 2 (noted as G_2) all W, Z bosons, scalar H boson, Goldstone bosons and ghost particles exchanging in the loop diagrams. As we shown later that one-loop contributing to the vertex HWW contains both ultraviolet divergent (UV-divergent) and infrared divergent (IR-divergent). The counter-terms for cancelling the UV-divergent are shown as diagram in group

G_0. To handle with the IR-divergent, we include the bremsstrahlung processes $H^* \to W^+W^-\gamma$ for both soft and hard photon contributions.

In general, one-loop contributions for the $H(p)W^+(q_1)W^-(q_2)$ vertex are expressed in terms of the Lorentz structure as follows:

$$\mathcal{V}^{1-\text{loop}}_{HW^+W^-} = g_{HWW}\Big\{F_{00}\, g^{\mu\nu} + \sum_{i,j=1}^{2} F_{ij}\, q_i^{\nu} q_j^{\mu} + iF\,\varepsilon_{\mu\nu\rho\sigma} q_1^{\rho} q_2^{\sigma}\Big\}. \tag{1}$$

Where $g_{HWW} = eM_W/s_W$ is the coupling of Higgs decay to W-pair. Here W boson mass is M_W and c_W (s_W) is cosine (sine) of Weinberg angle, respectively. In the vertex, the scalar functions F_{00}, F_{ij} for $i,j = 1,2$ and F are so-called one-loop form factors. They are functions of the momenta-squared as p^2, q_1^2, q_2^2. In this calculation, we use the `Package-X` [23] for handling all Dirac traces and Lorentz contractions in d dimensions. One-loop amplitudes are then decomposed into tensor one-loop integrals which are expressed in terms of the scalar PV-functions [24] in the standard notations of `LoopTools` [25]. As a result, one-loop form factors can be evaluated numerically by using this package.

In detail, analytical results for all form factors are shown in the following paragraphs. They are calculated as follows:

$$F_{00} = \sum_{G=\{G_0,G_1,G_2\}} F_{00}^{(G)} \tag{2}$$

with $\{G_0, G_1, G_2\} = \{\text{group 0}, \text{group 1}, \text{group 2}\}$ of Feynman diagrams. By considering the contributions of Feynman diagram in group 1, we have

$$\begin{aligned} F_{00}^{(G_1)} &= \frac{e^3}{(64\pi^2)s_W^3 M_W} N_t^C m_t^2 \Big\{ 2B_0(p^2, m_t^2, m_t^2) + B_0(q_1^2, m_b^2, m_t^2) + B_0(q_2^2, m_b^2, m_t^2) \\ &\quad + \Big[(2m_t^2 + m_b^2 - q_1^2 - q_2^2) C_0(p^2, q_1^2, q_2^2, m_t^2, m_t^2, m_b^2) - 8C_{00}(p^2, q_1^2, q_2^2, m_t^2, m_t^2, m_b^2)\Big]\Big\}. \end{aligned} \tag{3}$$

It is noted that we take top and bottom quarks in the loop diagrams as an example. Our results must be included all fermions contributing in one-loop diagrams. From the second group of Feynman diagrams, one arrives at

$$\begin{aligned} F_{00}^{(G_2)} &= \frac{e^3}{(128\pi^2)s_W^3 c_W^4 M_W} \Big\{ \Big[8M_W^2 c_W^6 (4d-7) + 4c_W^4 (M_H^2 + 2M_W^2 s_W^2)\Big] \\ &\qquad \times C_{00}(p^2, q_1^2, q_2^2, M_W^2, M_W^2, M_W^2) \\ &\quad + 4M_W^2 c_W^2 \Big[2c_W^4 (M_W^2 + M_Z^2) - 2M_W^2 s_W^2 c_W^2 - M_H^2 s_W^4 \\ &\quad + c_W^2 \Big((4c_W^2 + s_W^2)(q_1^2 + q_2^2) - p^2(5c_W^2 + 2s_W^2)\Big)\Big] C_0(p^2, q_1^2, q_2^2, M_W^2, M_W^2, M_W^2) \\ &\quad + 4c_W^2 \Big[\Big(M_H^2 + 4M_W^2(2d-3) - 2M_W^2\Big)c_W^2 + 2M_W^2 s_W^2\Big] C_{00}(p^2, q_1^2, q_2^2, M_W^2, M_W^2, M_W^2) \\ &\quad + 4M_W^2 \Big[2c_W^4 M_Z^2 + \Big(4(q_1^2 + q_2^2) - 5p^2\Big)c_W^4\Big] C_0(p^2, q_1^2, q_2^2, M_W^2, M_W^2, M_W^2) \\ &\quad + 32(d-2) M_W^2 s_W^2 c_W^4 C_{00}(p^2, q_1^2, q_2^2, M_W^2, M_W^2, 0) \end{aligned}$$

$$
\begin{aligned}
&+4M_W^2 s_W^2 c_W^4 \Big[(2M_W^2 - M_H^2) + 3(q_1^2 + q_2^2 - p^2)\Big] C_0(p^2, q_1^2, q_2^2, M_W^2, M_W^2, 0) \\
&+4c_W^4 \Big(M_H^2 + 2M_W^2\Big) C_{00}(p^2, q_1^2, q_2^2, M_W^2, M_W^2, M_H^2) - 8c_W^4 M_W^4 C_0(p^2, q_1^2, q_2^2, M_W^2, M_W^2, M_H^2) \\
&+12M_H^2 c_W^4 C_{00}(p^2, q_1^2, q_2^2, M_H^2, M_H^2, M_W^2) - 12M_W^2 M_H^2 c_W^4 C_0(p^2, q_1^2, q_2^2, M_H^2, M_H^2, M_W^2) \\
&-3M_H^2 c_W^4 B_0(p^2, M_H^2, M_H^2) - 4M_W^2 c_W^4 \Big[B_0(q_1^2, M_H^2, M_W^2) + B_0(q_2^2, M_H^2, M_W^2)\Big] \\
&+4M_W^2 c_W^2 \Big(c_W^4 + c_W^2 - s_W^4\Big) \Big[B_0(q_1^2, M_W^2, M_W^2) + B_0(q_2^2, M_W^2, M_W^2)\Big] \\
&-\Big[3M_H^2 c_W^4 - 8M_W^2 c_W^4 (d-2)\Big] B_0(p^2, M_W^2, M_W^2) \Bigg\}.
\end{aligned}
$$

As we show in the later, form factor F_{00} contains the UV-divergent. Following the renormalization theory, the counter-term ($F_{00}^{(G_0)}$) is given in Eq. (32). Other form factors can be given as follows:

$$
F_{ij} = \sum_{G=\{G_1,G_2\}} F_{ij}^{(G)} \tag{4}
$$

Applying the same procedure, one has analytic expression for F_{11} as

$$
\begin{aligned}
F_{11}^{(G_1)} = -\frac{e^3}{(32\pi^2) s_W^3 M_W} N_t^C m_t^2 \Big[& C_0(p^2, q_1^2, q_2^2, m_t^2, m_t^2, m_b^2) + 5C_1(p^2, q_1^2, q_2^2, m_t^2, m_t^2, m_b^2) \\
&+ 4C_{11}(p^2, q_1^2, q_2^2, m_t^2, m_t^2, m_b^2)\Big]
\end{aligned} \tag{5}
$$

and

$$
\begin{aligned}
F_{11}^{(G_2)} = \;& \frac{e^3}{(32\pi^2) s_W^3 c_W^2 M_W} \Bigg\{ M_W^2 c_W^2 (2c_W^2 + s_W^2) C_0(p^2, q_1^2, q_2^2, M_W^2, M_W^2, M_W^2) \\
&+c_W^2 \Big[4M_W^2 c_W^2 (2d-3) + M_H^2\Big] C_1(p^2, q_1^2, q_2^2, M_W^2, M_W^2, M_W^2) \\
&+c_W^2 \Big[2M_W^2 c_W^2 (4d-7) + M_H^2 + 2M_W^2 s_W^2\Big] C_{11}(p^2, q_1^2, q_2^2, M_W^2, M_W^2, M_W^2) \\
&+2M_W^2 C_0(p^2, q_1^2, q_2^2, M_W^2, M_W^2, M_W^2) \\
&+\Big[M_H^2 c_W^2 + 4M_W^2 c_W^2 (2d-3) + 3M_W^2 s_W^2\Big] C_1(p^2, q_1^2, q_2^2, M_W^2, M_W^2, M_W^2) \\
&+\Big[M_H^2 c_W^2 + 2M_W^2 c_W^2 (4d-7) + 2M_W^2 s_W^2\Big] C_{11}(p^2, q_1^2, q_2^2, M_W^2, M_W^2, M_W^2) \\
&+2c_W^2 M_W^2 C_0(p^2, q_1^2, q_2^2, M_W^2, M_W^2, M_H^2) + c_W^2 \Big(M_H^2 + 3M_W^2\Big) C_1(p^2, q_1^2, q_2^2, M_W^2, M_W^2, M_H^2)
\end{aligned} \tag{6}
$$

$$
\begin{aligned}
&+c_W^2\left(M_H^2+2M_W^2\right)C_{11}(p^2,q_1^2,q_2^2,M_W^2,M_W^2,M_H^2)\\
&+3M_H^2c_W^2\Big[C_1(p^2,q_1^2,q_2^2,M_H^2,M_H^2,M_W^2)+C_{11}(p^2,q_1^2,q_2^2,M_H^2,M_H^2,M_W^2)\Big]\\
&+M_W^2s_W^2c_W^2\Big[C_0(p^2,q_1^2,q_2^2,M_W^2,M_W^2,0)+(8d-12)C_1(p^2,q_1^2,q_2^2,M_W^2,M_W^2,0)\\
&\qquad\qquad+(8d-16)C_{11}(p^2,q_1^2,q_2^2,M_W^2,M_W^2,0)\Big]\Bigg\}.
\end{aligned}
$$

Analytical formulas for F_{22} are shown accordingly

$$
F_{22}^{(G_1)} = -\frac{e^3N_t^Cm_t^2}{(32\pi^2)s_W^3M_W}\Big[C_1(p^2,q_2^2,q_1^2,m_t^2,m_t^2,m_b^2)+4C_{11}(p^2,q_2^2,q_1^2,m_t^2,m_t^2,m_b^2)\Big], \tag{7}
$$

$$
\begin{aligned}
F_{22}^{(G_2)} &= \frac{e^3}{(32\pi^2)s_W^3c_W^2M_W}\Bigg\{3M_H^2c_W^2C_{11}(p^2,q_2^2,q_1^2,M_H^2,M_H^2,M_W^2) \\
&+M_W^2s_W^2c_W^2C_0(p^2,q_2^2,q_1^2,M_W^2,M_W^2,M_W^2)+2M_W^2c_W^4C_1(p^2,q_2^2,q_1^2,M_W^2,M_W^2,M_W^2)\\
&+c_W^2\Big[2c_W^2M_W^2(4d-7)+(M_H^2+2M_W^2s_W^2)\Big]C_{11}(p^2,q_2^2,q_1^2,M_W^2,M_W^2,M_W^2)\\
&+M_W^2(2c_W^2+s_W^2)C_1(p^2,q_2^2,q_1^2,M_W^2,M_W^2,M_W^2)\\
&+\Big[c_W^2\Big(2M_W^2(4d-7)+M_H^2\Big)+2M_W^2s_W^2\Big]C_{11}(p^2,q_2^2,q_1^2,M_W^2,M_W^2,M_W^2)\\
&+c_W^2\Big[M_W^2C_1(p^2,q_2^2,q_1^2,M_W^2,M_W^2,M_H^2)+(M_H^2+2M_W^2)C_{11}(p^2,q_2^2,q_1^2,M_W^2,M_W^2,M_H^2)\Big]\\
&+M_W^2s_W^2c_W^2\Big[8(d-2)C_{11}(p^2,q_2^2,q_1^2,M_W^2,M_W^2,0)+2C_1(p^2,q_2^2,q_1^2,M_W^2,M_W^2,0)\\
&-C_0(p^2,q_2^2,q_1^2,M_W^2,M_W^2,0)\Big]\Bigg\}.
\end{aligned} \tag{8}
$$

The form factor F_{12} is given by

$$
F_{12}^{(G_1)} = \frac{e^3}{(8\pi^2)s_W^3M_W}N_t^Cm_t^2\Big[C_1(p^2,q_2^2,q_1^2,m_t^2,m_t^2,m_b^2)+C_{12}(q_1^2,p^2,q_2^2,m_b^2,m_t^2,m_t^2)\Big] \tag{9}
$$

and

$$
\begin{aligned}
F_{12}^{(G_2)} &= \frac{e^3}{(32\pi^2)s_W^3c_W^2M_W}\Bigg\{c_W^2\Big[2M_W^2c_W^2(7-4d)-(M_H^2+6M_W^2s_W^2)\Big]\times\\
&\qquad\times C_1(p^2,q_2^2,q_1^2,M_W^2,M_W^2,M_W^2)\\
&-2M_W^2s_W^2c_W^2\Big[2C_0(p^2,q_1^2,q_2^2,M_W^2,M_W^2,M_W^2)+3C_1(p^2,q_1^2,q_2^2,M_W^2,M_W^2,M_W^2)\Big]\\
&+\Big[2M_W^2c_W^2(7-4d)-(M_H^2c_W^2+M_W^2s_W^2)\Big]C_1(p^2,q_2^2,q_1^2,M_W^2,M_W^2,M_W^2)
\end{aligned} \tag{10}
$$

$$
\begin{aligned}
&+M_W^2 s_W^2\Big[C_0(p^2,q_1^2,q_2^2,M_W^2,M_W^2,M_W^2)+C_1(p^2,q_1^2,q_2^2,M_W^2,M_W^2,M_W^2)\Big]\\
&+\Big[2M_W^2c_W^2(7-4d)-(M_H^2c_W^2+2M_W^2s_W^2)\Big]C_{12}(q_1^2,p^2,q_2^2,M_W^2,M_W^2,M_W^2)\\
&+2M_W^2s_W^2c_W^2\Big[2C_0(p^2,q_1^2,q_2^2,M_W^2,M_W^2,0)+3C_1(p^2,q_1^2,q_2^2,M_W^2,M_W^2,0)\\
&-(4d-10)C_1(p^2,q_2^2,q_1^2,M_W^2,M_W^2,0)\Big]\\
&+M_W^2c_W^2\Big[C_0(p^2,q_1^2,q_2^2,M_W^2,M_W^2,M_H^2)+C_1(p^2,q_1^2,q_2^2,M_W^2,M_W^2,M_H^2)\\
&-8s_W^2(d-2)C_{12}(q_1^2,p^2,q_2^2,0,M_W^2,M_W^2)\Big]\\
&-c_W^2\Big[(M_H^2+M_W^2)C_1(p^2,q_2^2,q_1^2,M_W^2,M_W^2,M_H^2)+(M_H^2+2M_W^2)C_{12}(q_1^2,p^2,q_2^2,M_H^2,M_W^2,M_W^2)\Big]\\
&-3M_H^2c_W^2\Big[C_1(p^2,q_2^2,q_1^2,M_H^2,M_H^2,M_W^2)+C_{12}(q_1^2,p^2,q_2^2,M_W^2,M_H^2,M_H^2)\Big]\\
&-\Big[M_H^2c_W^2+2M_W^2c_W^2\Big((4d-7)c_W^2+s_W^2\Big)\Big]C_{12}(q_1^2,p^2,q_2^2,M_W^2,M_W^2,M_W^2)\Bigg\}.
\end{aligned}
$$

Next form factor F_{21} is shown

$$
\begin{aligned}
F_{21}^{(G_1)} &= \frac{e^3\,N_t^C m_t^2}{(32\pi^2)s_W^3M_W}\Big[C_1(p^2,q_1^2,q_2^2,m_t^2,m_t^2,m_b^2)+C_1(p^2,q_2^2,q_1^2,m_t^2,m_t^2,m_b^2)\\
&\qquad +4C_{12}(q_1^2,p^2,q_2^2,m_b^2,m_t^2,m_t^2)\Big]. \qquad (11)
\end{aligned}
$$

$$
\begin{aligned}
F_{21}^{(G_2)} &= \frac{e^3}{(32\pi^2)s_W^3c_W^2M_W}\Bigg\{2M_W^2c_W^2\Big[4C_0(p^2,q_1^2,q_2^2,M_W^2,M_W^2,M_W^2)\\
&\qquad +(3s_W^2-c_W^2)C_1(p^2,q_1^2,q_2^2,M_W^2,M_W^2,M_W^2)\Big]\\
&+2M_W^2c_W^2\Big(3s_W^2-c_W^2\Big)C_1(p^2,q_2^2,q_1^2,M_W^2,M_W^2,M_W^2)\\
&+\Big[2M_W^2c_W^2(7-4d)-(M_H^2c_W^2+2M_W^2s_W^2)\Big]C_{12}(q_1^2,p^2,q_2^2,M_W^2,M_W^2,M_W^2)\\
&+2M_W^2\Big[4c_W^2C_0(p^2,q_1^2,q_2^2,M_W^2,M_W^2,M_W^2)-C_1(p^2,q_1^2,q_2^2,M_W^2,M_W^2,M_W^2)\Big]\\
&-2M_W^2C_1(p^2,q_2^2,q_1^2,M_W^2,M_W^2,M_W^2)+8M_W^2s_W^2c_W^2(2-d)C_{12}(q_1^2,p^2,q_2^2,0,M_W^2,M_W^2)\\
&-8M_W^2s_W^2c_W^2\Big[C_1(p^2,q_1^2,q_2^2,M_W^2,M_W^2,0)+C_1(p^2,q_2^2,q_1^2,M_W^2,M_W^2,0)\Big]\\
&-2M_W^2c_W^2\Big[C_1(p^2,q_1^2,q_2^2,M_W^2,M_W^2,M_H^2)+C_1(p^2,q_2^2,q_1^2,M_W^2,M_W^2,M_H^2)\Big]\\
&-(M_H^2+2M_W^2)c_W^2C_{12}(q_1^2,p^2,q_2^2,M_H^2,M_W^2,M_W^2)\\
&-3M_H^2c_W^2C_{12}(q_1^2,p^2,q_2^2,M_W^2,M_H^2,M_H^2)\\
&-c_W^2\Big[M_H^2+2M_W^2\Big(c_W^2(4d-7)+s_W^2\Big)\Big]C_{12}(q_1^2,p^2,q_2^2,M_W^2,M_W^2,M_W^2)\Bigg\}. \qquad (12)
\end{aligned}
$$

The form factor F (the coefficient of Levi Civita) is written as

$$\begin{aligned} F &= -\frac{e^3 N_t^C m_t^2}{(32\pi^2) s_W^3 M_W \Big[p^4 - 2p^2(q_1^2+q_2^2) + (q_1^2-q_2^2)^2\Big]} \times \\ &\quad \times \Bigg\{ (q_1^2 - q_2^2)\Big[\Big(2m_t^2 + m_b^2 - p^2 + q_1^2 + q_2^2\Big) C_0(p^2, q_1^2, q_2^2, m_t^2, m_t^2, m_b^2) - 2B_0(p^2, m_t^2, m_t^2)\Big] \\ &\quad + \Big(p^2 - q_1^2 - 3q_2^2\Big) B_0(q_2^2, m_b^2, m_t^2) - \Big(p^2 - 3q_1^2 - q_2^2\Big) B_0(q_1^2, m_b^2, m_t^2) \Bigg\}. \end{aligned} \tag{13}$$

In the case of both external W-bosons are on-shell masses $q_1^2 = q_2^2 = M_W^2$, the form factor F is canceled analytically in our calculations.

2.1. One-loop virtual $H^* \to WW$

We turn out attention to the one-loop amplitude for off-shell $H^* \to W^+W^-$. All one-loop virtual, soft and hard bremsstrahlung contributions are taken into account in the current calculation. For one-loop virtual contributions, the amplitude is written in the form of

$$\mathscr{M}^{1-\text{loop}}_{H^*\to WW} = g_{HWW} \Big\{ F_{00,H^*\to WW}\, g^{\mu\nu} + F_{21,H^*\to WW}\, q_2^\mu q_1^\nu \Big\} \epsilon_\mu^*(q_1) \epsilon_\nu^*(q_2). \tag{14}$$

Where ϵ_μ, ϵ_ν are polarization vectors for final W bosons. Since one considers two real W bosons in final state, we have only F_{00}, F_{21} contributing to the amplitude. Analytic expressions for these form factors can be written as follows:

$$F_{00,H^*\to WW} = F_{00}(p^2; M_W^2, M_W^2) = \sum_{G=\{G_0,G_1,G_2\}} F_{00}^{(G)}(p^2; M_W^2, M_W^2), \tag{15}$$

$$F_{21,H^*\to WW} = F_{21}(p^2; M_W^2, M_W^2) = \sum_{G=\{G_1,G_2\}} F_{21}^{(G)}(p^2; M_W^2, M_W^2). \tag{16}$$

One-loop virtual off-shell decay rates for $H^* \to WW$ are calculated in terms of the above form factors as follows. Following kinematic variables $p^2 = M_{WW}^2, q_1^2 = M_W^2$ and $q_2^2 = M_W^2$ are used. For tree-level decay rates, we have

$$\Gamma_{\text{tree}} = g_{HWW}^2 \frac{\sqrt{M_{WW}^2 - 4M_W^2}}{64\pi M_W^4 M_{WW}^2} (12M_W^4 - 4M_W^2 M_{WW}^2 + M_{WW}^4). \tag{17}$$

One-loop virtual decay rates are given by

$$\begin{aligned} \Gamma_{\text{1-loop}} &= g_{HWW}^2 \frac{\sqrt{M_{WW}^2 - 4M_W^2}}{64\pi M_W^4 M_{WW}^2} \Bigg\{ (24M_W^4 - 8M_W^2 M_{WW}^2 + 2M_{WW}^4) \mathscr{R}e[F_{00,H^*\to WW}] \\ &\quad + M_{WW}^2 (8M_W^4 - 6M_W^2 M_{WW}^2 + M_{WW}^4) \mathscr{R}e[F_{21,H^*\to WW}] \Bigg\}. \end{aligned} \tag{18}$$

2.2. Soft photon contribution for $H^* \to W^+W^-\gamma_S$

In order to regular IR-divergent, we have to include the soft contribution which is corresponding to the decay process $H^*(p) \to W^+_\mu(q_1)W^-_\nu(q_2)\gamma_\rho(q_3)$. The decay rates for the soft-photon contributions can be factorized as follows:

$$\Gamma_{\text{soft}} = \delta_{\text{soft}}\Gamma_{\text{tree}} \tag{19}$$

where Γ_{tree} is decay rates of $H^*(p) \to W^+_\mu(q_1)W^-_\nu(q_2)$ at tree-level. The soft factor δ_s depends on the infrared regulator of photon mass λ and photon energy cut-off k_c is given [24]:

$$\delta_{\text{soft}} = -\frac{\alpha}{4\pi^2}\int\limits_{\lambda\le E_\gamma\le k_c}\frac{d^3q_3}{E_\gamma}\Big(\frac{q_1}{q_1\cdot q_3}-\frac{q_2}{q_2\cdot q_3}\Big)^2 = -\frac{\alpha}{4\pi^2}\Big[I_{11}+I_{22}-2I_{12}\Big], \tag{20}$$

where photon energy $E_\gamma = \sqrt{|q_3|^2+\lambda^2}$. The basic integrals I_{ij} are given

$$I_{11} = I_{22} = (2\pi)\Bigg\{\ln\frac{4k_c^2}{\lambda^2}+\frac{1}{\beta}\ln\Big[\frac{1-\beta}{1+\beta}\Big]\Bigg\}, \tag{21}$$

$$I_{12} = \frac{(2\pi)}{\beta}\Bigg[\beta^2+\frac{2M_W^2}{M_{WW}^2}\Bigg]\Bigg\{\ln\Big[\frac{1+\beta}{1-\beta}\Big]\ln\frac{4k_c^2}{\lambda^2}-2\mathrm{Li}_2\Big[\frac{2\beta}{1+\beta}\Big]-\frac{1}{2}\ln^2\Big[\frac{1+\beta}{1-\beta}\Big]\Bigg\} \tag{22}$$

where $\beta = \sqrt{1-4M_W^2/M_{WW}^2}$.

2.3. Hard photon contribution for $H^* \to W^+W^-\gamma_H$

We next consider the hard-photon contribution in this subsection. The corresponding decay process is $H^*(p) \to W^+_\mu(q_1)W^-_\nu(q_2)\gamma_\rho(q_3)_H$ which γ_H is the hard photon in final state. All tree-level Feynman diagrams are plotted in Fig. 1.

The squared amplitude is shown in terms of the Mandelstam variables $s=(q_1+q_2)^2, t=(q_2+q_3)^2, u=(q_1+q_3)^2$ as follows:

$$\begin{aligned}\sum_{\text{pol}}|\mathscr{M}_{\text{hard}}|^2 = \;& \frac{e^4M_W^2}{M_W^2(M_{WW}^2-M_W^2)(M_W^2-t)^2(M_W^2-u)^2}\times \\ &\times\Bigg\{80M_W^{10}-8M_W^8(7s+12(t+u))+4M_W^6\Big[3s^2+18s(t+u)+4(2t+u)(t+2u)\Big] \\ &-M_W^4\Big[s^3+(14s^2+16tu)(t+u)+s(25t^2+74tu+25u^2)\Big]-stu(s+t+u)^2 \\ &+M_W^2\Big[s^3(t+u)+s(s+t+u)(3t^2+14tu+3u^2)-(t^2-u^2)^2\Big]\Bigg\}.\end{aligned} \tag{23}$$

The Mandelstam invariants follow $s+t+u = M_{WW}^2+2M_W^2$. The decay rates are calculated accordingly

$$\Gamma_{\text{hard}} = \frac{1}{256\pi^3M_{WW}^3}\int\limits_{4M_W^2}^{M_{WW}(M_{WW}-2k_c)} ds\int\limits_{t_{\min}}^{t_{\max}} dt\sum_{\text{pol}}|\mathscr{M}_{\text{hard}}|^2, \tag{24}$$

where

$$t_{\max,\min} = \frac{1}{2}\left\{M_{WW}^2 + 2M_W^2 - s \pm \sqrt{\left(1-\frac{4M_W^2}{s}\right)\left[(M_{WW}^2 - s)^2\right]}\right\}. \tag{25}$$

Having all the contributions, the total decay rate is given

$$\Gamma^{\text{total}}_{H^*\to W^+W^-} = \Gamma_{\text{tree}} + \Gamma_{\text{1-loop}} + \Gamma_{\text{soft}} + \Gamma_{\text{hard}}. \tag{26}$$

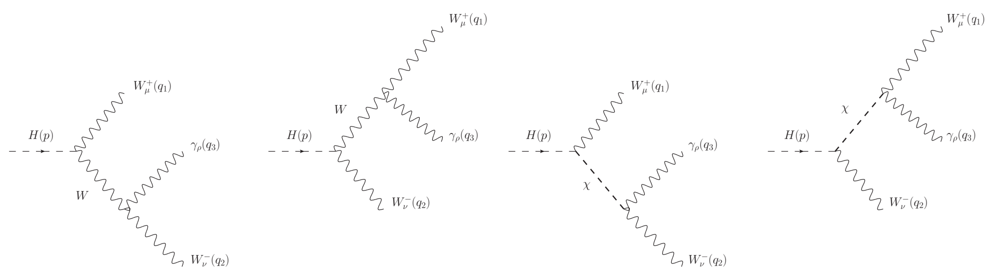

Fig. 1. Tree-level Feynman diagrams for hard photon contribution

3. Phenomenological results

For studying physical results, we use the input parameters as follows. All boson masses are taken: $M_Z = 91.1876$ GeV, $\Gamma_Z = 2.4952$ GeV, $M_W = 80.379$ GeV, $\Gamma_W = 2.085$ GeV, $M_H = 125$ GeV, $\Gamma_H = 4.07\cdot 10^{-3}$ GeV. For lepton sectors, their masses are selected: $m_e = 0.00052$ GeV, $m_\mu = 0.10566$ GeV and $m_\tau = 1.77686$ GeV. All quark masses are given by $m_u = 0.00216$ GeV $m_d = 0.0048$ GeV, $m_c = 1.27$ GeV, $m_s = 0.93$ GeV, $m_t = 173.0$ GeV, and $m_b = 4.18$ GeV. In this paper, we work in the so-called G_μ-scheme. In this scheme, one takes the Fermi constant as input parameter getting $G_\mu = 1.16638\cdot 10^{-5}$ GeV^{-2}. Subsequently, the electroweak coupling can be then evaluated by

$$\alpha = \sqrt{2}/\pi G_\mu M_W^2(1 - M_W^2/M_Z^2) = 1/132.184. \tag{27}$$

3.1. Decay rates of off-shell $H^*\to W^+W^-$

We first evaluate decay rates of off-shell $H^*\to W^+W^-$. In Fig. 2, we present decay rates of off-shell $H^*\to W^+W^-$ as a function of M_{WW}. Off-shell Higgs mass M_{WW} is range of 200 GeV to 500 GeV. In the left panel, tree-level contribution to decay rates is presented as solid line. Total one-loop radiative corrections to the decay rates in the case of unpolarized for W bosons is plotted as dashed-line and in the case of longitudinal polarizations for W bosons is shown as dash-dotted line, respectively. In the right panel, we show the one-loop radiative corrections in percentage to the decay rates. The corrections are defined as follows:

$$\delta[\%] = \frac{\Gamma^{\text{total}}_{H^*\to WW} - \Gamma^{\text{tree}}_{H^*\to WW}}{\Gamma^{\text{tree}}_{H^*\to WW}} \times 100\%. \tag{28}$$

We find that the corrections are range form 5% to 15% for the unpolarized case for W bosons and from -80% to 10% for the longitudinal polarization case for W bosons, respectively. The corrections are massive contributions. They must be taken into account at future colliders.

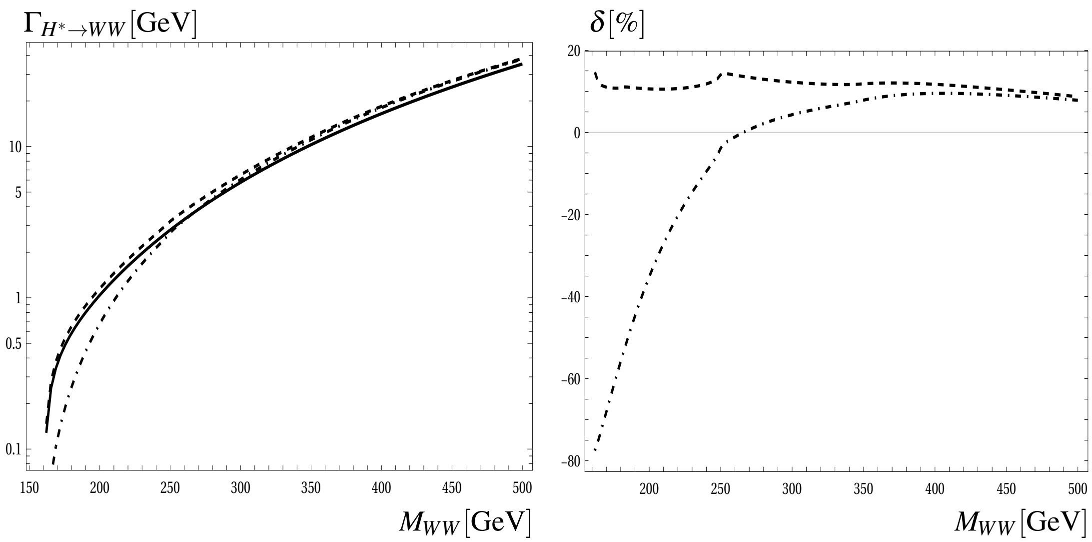

Fig. 2. Off-shell Higgs decay rates as a function of M_{WW}.

3.2. *Off-shell $H^* \to W^+W^-$ in Higgs processes at future colliders*

The effects of one-loop off-shell $H^* \to W^+W^-$ in Higgs processes at future lepton colliders are discussed in this section. It is well-known that three main Higgs productions at future lepton colliders, for example, $e^-e^+ \to ZH^* \to Z(WW)$ and $e^-e^+ \to f\bar{f}H^* \to f\bar{f}(WW)$ for $f = e, \nu_e$. Since dominant cross sections of $e^-e^+ \to ZH^* \to Z(WW)$ and $e^-e^+ \to \nu_e\bar{\nu}_eH^* \to \nu_e\bar{\nu}_e(WW)$ in comparision with $e^-e^+ \to e^-e^+H^* \to e^-e^+(WW)$ at the ILC, we only shown numerical results for the signals of the former processes. All the signals are presented including initial beam polarization at future lepton colliders. In detail, production cross sections are derived according to

$$\frac{d\sigma^{e^-e^+\to VH^*\to V(WW)}(\sqrt{s})}{dM_{WW}} = \frac{2M_{WW}^2}{\pi}\,\frac{\sigma^{e^-e^+\to VH^*}(\sqrt{s},M_{WW})\times\Gamma_{H^*\to WW}(M_{WW})}{[(M_{WW}^2-M_H^2)^2+\Gamma_H^2M_H^2]} \tag{29}$$

for $V \equiv Z, f\bar{f}$ with $f \equiv e^-, \nu_e$. For deriving the above formulas, we refer our previous work for more detail [26, 27]. The total cross sections then read:

$$\sigma^{e^-e^+\to V(WW)}(\sqrt{s}) = \int\limits_{2M_W}^{\sqrt{s}-M_V} dM_{WW}\,\frac{2M_{WW}^2}{\pi}\,\frac{\sigma^{e^-e^+\to VH^*}(\sqrt{s},M_{WW})\times\Gamma_{H^*\to WW}(M_{WW})}{[(M_{WW}^2-M_H^2)^2+\Gamma_H^2M_H^2]}. \tag{30}$$

In Fig. 3, the differential cross sections for the production $e^-e^+ \to ZH^* \to Z(WW)$ as functions of off-shell Higgs mass M_{WW} are plotted at center-of-mass energy $\sqrt{s} = 500$ GeV and at $\sqrt{s} = 1000$ GeV. In the left (right) panel, we show for *LR* (*RL*) polarization of e^-, e^+ beams, respectively. In these Figures, the solid line is for tree-level contributions. The dashed line presents for full one-loop radiative corrections decay rates in the case of unpolarized W-pair in the final state. While the dash-dotted line shows for full one-loop radiative corrections decay rates with longitudinal polarization for W-pair. The cross sections increase up to the threshold $M_{WW} \sim 180$ GeV (for

$\sqrt{s} = 500$ GeV) and $M_{WW} \sim 400$ GeV (for $\sqrt{s} = 1000$ GeV), they decrease rapidly beyond the peaks. We find that one-loop corrections to off-shell Higgs decay are visible impacts (specially, in the lower regions of off-shell Higgs mass) in these distributions. In Fig. 3, the differential cross

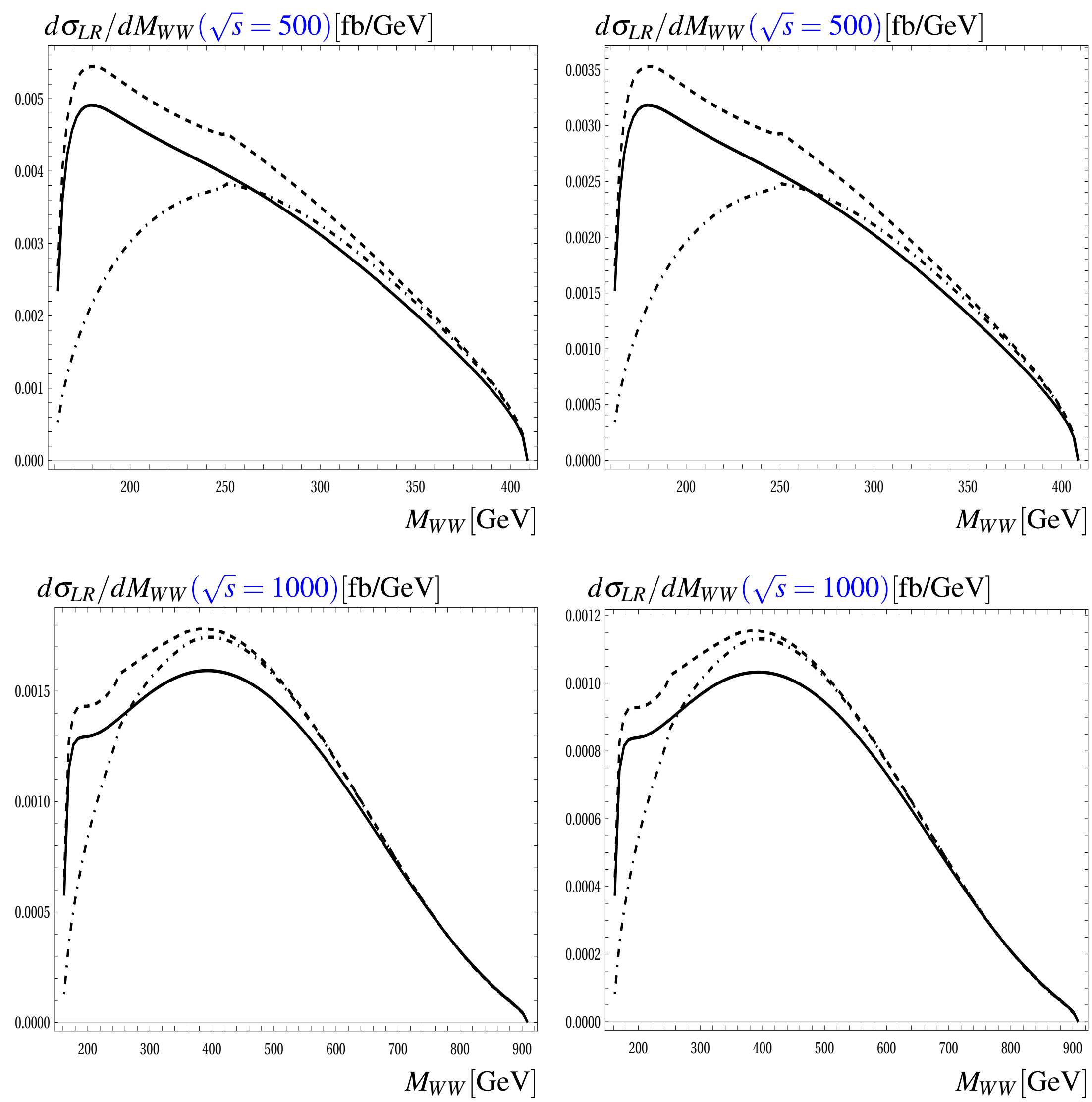

Fig. 3. Differential cross sections as a function of M_{WW}.

sections for the production $e^-e^+ \to \nu_e\bar{\nu}_e H^* \to \nu_e\bar{\nu}_e(WW)$ as functions of off-shell Higgs mass M_{WW} are generated at $\sqrt{s} = 500$ GeV (left panel) and at $\sqrt{s} = 1000$ GeV (right panel), respectively. We use the same previous notations. We observe a peak around the threshold $M_{WW} = 2M_W \sim 180$ GeV. The cross sections develop to the peak and decrease rapidly beyond the peak.

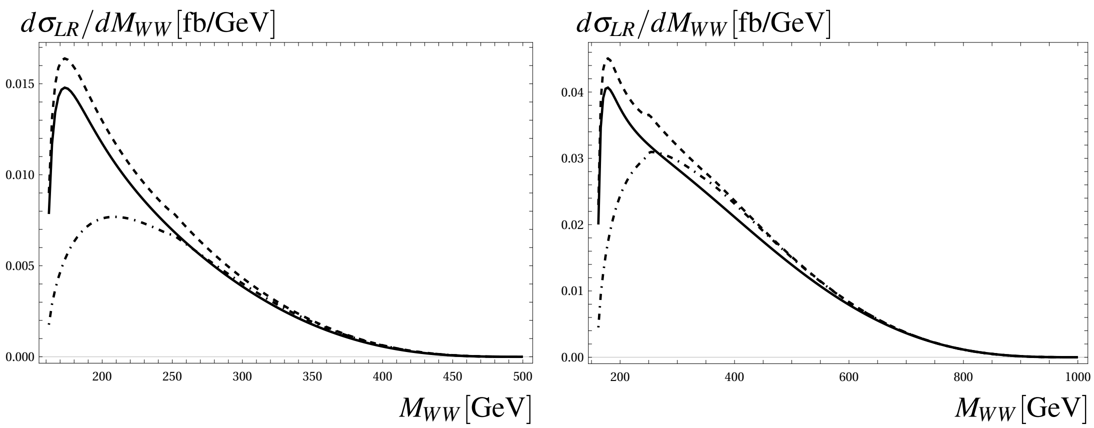

Fig. 4. Differential cross sections as a function of M_{WW}.

We turn our attention to the Higgs production at future e^--γ colliders. The signal cross section is written as follows

$$\begin{aligned}\frac{d^2\sigma(\sqrt{s},Q^2)}{dM_{WW}\,dQ^2} &= \frac{e^2}{16\pi s}\left[\frac{s^2+(M_{WW}^2-Q^2-s)^2}{Q^2(s^2-Q^2)^2}\right]\times\left|F_{00}^{H^*\to\gamma^*\gamma}(s,Q^2,0)\right|^2\times\\ &\quad\times\frac{2M_{WW}}{[(M_{WW}^2-M_H^2)^2+\Gamma_H^2M_H^2]}\times\frac{M_{WW}\,\Gamma_{H^*\to WW}(M_{WW})}{\pi}. \qquad (31)\end{aligned}$$

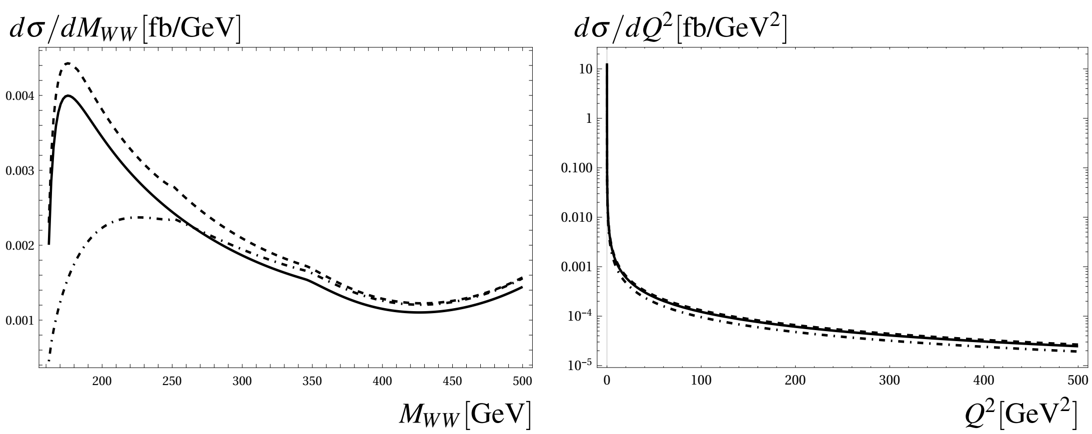

Fig. 5. Differential cross sections as a function of M_{WW} and Q^2.

In Fig. 5, we present the differential cross sections with respect to the off-shell Higgs mass M_{WW} (left panel) and Q^2 (right panel). In the left figure (Fig. 5), we find the same previous conclusions. In the right Figure, the cross-section is dominant in the low region of Q^2 in comparision with higher-region of Q^2. With high-luminosity at future colliders, the signal cross sections could be probed in the future. The effects of one-loop corrections to the off-shell play important roles in this analysis for testing the SM at higher-energy and for extracting new physic signals.

4. Conclusions

In this paper, we have presented full one-loop radiative corrections to off-shell decay $H^* \to W^+W^-$ in the 't Hooft-Veltman in framework of the SM. One-loop form factors for decay process are written in terms of the PV-functions in the standard notations of `LoopTools`. As a result, the off-shell decay rates can be computed numerically by using this program. In phenomenological results, we have shown the decay rates and one-loop corrections as functions of the off-shell Higgs mass. The corrections are range of 5% to 15% for the unpolarized case for W bosons and of -80% to 10% for the longitudinal polarization case for W bosons, respectively. In applications, we have examined the impacts of one-loop corrections to off-shell decay $H^* \to W^+W^-$ in Higgs processes at future colliders.The signal processes such as $e^-e^+ \to ZH^* \to Z(WW)$ and $e^-e^+ \to \nu_e\bar{\nu}_e H^* \to \nu_e\bar{\nu}_e(WW)$ and $e^-\gamma \to e^-H^* \to e^-WW$ are examined. We find that the effects are visible impacts and these should be taken into account at future colliders.

Acknowledgment

This research is funded by Vietnam National University, Ho Chi Minh City (VNU-HCM) under grant number C2022-18-14.

References

[1] ATLAS Collaboration, *Physics at a high-luminosity LHC with ATLAS*, arXiv:1307.7292.
[2] CMS Collaboration, *Projected performance of an upgraded CMS detector at the LHC and HL-LHC: contribution to the snowmass process*, arXiv:1307.7135.
[3] H. Baer, T. Barklow, K. Fujii, Y. Gao, A. Hoang, S. Kanemura *et al.*, *The international linear collider technical design report - Volume 2: Physics*, arXiv:1306.6352.
[4] CDF and D0 Collaborations, *Combination of Tevatron Searches for the Standard Model Higgs Boson in the W^+W^- Decay Mode*, Phys. Rev. Lett. **104** (2010) 061802.
[5] CMS Collaboration, *Measurement of W^+W^- production and search for the Higgs boson in pp collisions at $\sqrt{s} = 7$ TeV*, Phys. Lett. B **699** (2011) 25.
[6] [CMS Collaboration] S. Chatrchyan *et al.*, *Search for the standard model Higgs boson decaying to W^+W^- in the fully leptonic final state in pp collisions at $\sqrt{s} = 7$ TeV*, Phys. Lett. B **710** (2012) 91.
[7] ATLAS Collaboration, *Search for the Higgs boson in the $H \to WW$ decay channel in pp collisions at $\sqrt{s} = 7$ TeV with the ATLAS detector*, Phys. Rev. Lett. **108** (2012) 111802.
[8] CMS Collaboration, *Measurement of Higgs boson production and properties in the WW decay channel with leptonic final states*, J. High Energ. Phys. **01** (2014) 096.
[9] ATLAS Collaboration, *Study of (W/Z)H production and Higgs boson couplings using $H \to WW^*$ decays with the ATLAS detector*, J. High Energ. Phys. **08** (2015) 137.
[10] ATLAS Collaboration, *Measurement of the production cross section for a Higgs boson in association with a vector boson in the $H \to WW^*$ channel in pp collisions at $\sqrt{s}$ = 13 TeV with the ATLAS detector*, Phys. Lett. B **798** (2019) 134949.
[11] CMS Collaboration, *Measurements of the Higgs boson production cross section and couplings in the W boson pair decay channel in proton-proton collisions at $\sqrt{s}$ = 13 TeV*, Eur. Phys. J. C **83** (2023) 667.
[12] ATLAS Collaboration, *Measurements of Higgs boson production by gluon−gluon fusion and vector-boson fusion using $H \to WW^* \to e\nu\mu\nu$ decays in pp collisions at $\sqrt{s} = 13$ TeV with the ATLAS detector*, arXiv:2207.00338.
[13] ATLAS Collaboration, *Measurement of the Higgs boson production cross section in association with a vector boson and decaying into WW^* with the ATLAS detector at $\sqrt{s} = 13$ TeV*, ATLAS-CONF-2022-067.
[14] B. A. Kniehl, *Radiative corrections for $H \to W^+W^-$ (γ) in the standard model*, Nucl. Phys. B **357** (1991) 439.

[15] C. Ma, Y. Wang, X. Xu, L. L. Yang and B. Zhou, *Mixed QCD-EW corrections for Higgs leptonic decay via HW^+W^- vertex*, J. High Energ. Phys. **09** (2021) 114.
[16] B. A. Kniehl and O. L. Veretin, *Low-mass Higgs decays to four leptons at one loop and beyond*, Phys. Rev. D **86** (2012) 053007.
[17] A. Bredenstein, A. Denner, S. Dittmaier and M. M. Weber, *Precise predictions for the Higgs-boson decay $H \to WW, ZZ \to 4$ leptons*, Phys. Rev. D **74** (2006) 013004.
[18] A. Bredenstein, A. Denner, S. Dittmaier and M. M. Weber, *Radiative corrections to the semileptonic and hadronic Higgs-boson decays $H \to WW, ZZ \to 4$ leptons*, J. High Energ. Phys. **02** (2007) 080.
[19] W. Hollik and J. H. Zhang, *Radiative Corrections to $H^0 \to WW/ZZ$ in the MSSM*, Phys. Rev. D **84** (2011) 055022.
[20] L. Altenkamp, M. Boggia and S. Dittmaier, *Precision calculations for $h \to WW/ZZ \to 4$ fermions in a Singlet Extension of the Standard Model with Prophecy4f*, J. High Energ. Phys. **04** (2018) 062.
[21] L. Altenkamp, S. Dittmaier and H. Rzehak, *Precision calculations for $h \to WW/ZZ \to 4$ fermions in the Two-Higgs-Doublet Model with Prophecy4f*, J. High Energ. Phys. **03** (2018) 110.
[22] L. Altenkamp, S. Dittmaier and H. Rzehak, *Renormalization schemes for the Two-Higgs-Doublet Model and applications to $h \to WW/ZZ \to 4$ fermions*, J. High Energ. Phys. **09** (2017) 134.
[23] H. H. Patel, *Package-X: A Mathematica package for the analytic calculation of one-loop integrals*, Comput. Phys. Commun. **197** (2015) 276.
[24] A. Denner and S. Dittmaier, *Reduction schemes for one-loop tensor integrals*, Nucl. Phys. B **734** (2006) 62.
[25] T. Hahn and M. Perez-Victoria, *Automatized one loop calculations in four-dimensions and D-dimensions*, Comput. Phys. Commun. **118** (1999) 153.
[26] K. H. Phan and D. T. Tran, *One-loop formulas for off-shell decay $H^* \to ZZ$ in 't Hooft-Veltman gauge and its applications*, arXiv:2209.12410.
[27] A. T. Nguyen, D. T. Tran and K. H. Phan, *One-loop on-shell and off-shell decay $H^* \to VV$ at future e^-e^- collider*, arXiv:2209.13153.
[28] D. T. Tran and K. H. Phan, *One-loop formulas for $H \to Z\nu_l\bar{\nu}_l$ for $l = e, \mu, \tau$ in 't Hooft-Veltman gauge*, Chinese Phys. C **47** (2023) 053106.

Appendix A: Numerical checks

In order to confirm the analytic results presenting in this paper, we first check the UV-finiteness of the results. It is mentioned in the previous section, the form factors $F_{00}^{(G_j)}$ for $j = 1,2,3$ contain UV-divergent. To regularize UV-divergent, counter-term form factor $F_{00}^{(G_0)}$ is taken into account (seen Eq. (32) for its analytical formulas). The numerical results for this check are presented in the following Table 1. In this Table, we change C_{UV}, μ^2 and we verify that the total form factor F_{00} is very good stability (over 11 digits).

Appendix B: Counter term

Counter-term of $H \cdot W_\mu^+ \cdot W_\nu^-$ vertex is taken the form of

$$F_{00}^{(G_0)} = g_{HWW}\big(\delta Y + \delta G_2 + \delta G_W + 2\delta Z_W^{1/2} + \delta Z_H^{1/2}\big). \tag{32}$$

All the renormalization constants presented in the above formulas can be found in [28].

Appendix C: Feynman diagrams

We show all Feynman diagrams for this decay process in 't Hooft-Veltman gauge in this appendix.

Table 1. Checking for the UV-finiteness of the results at $M_{WW} = 250$ GeV ($p^2 = M_{WW}^2$). In this case, two real bosons are considered in final state.

(C_{UV}, μ^2)	$\sum_{j=1}^{2} F_{00}^{(G_j)}$ $F_{00}^{(G_0)}$ $F_{00} = \sum_{j=0}^{2} F_{00}^{(G_j)}$
$(0,1)$	$-14447.359832765836 + 10323.270102389799\,i$ $14595.587461604524 + 0\,i$ $148.22762883868745 + 10323.270102389799\,i$
$(10^2, 10^4)$	$100549.21840082797 + 10323.270102389799\,i$ $-100400.99077198938 + 0\,i$ $148.22762883868804 + 10323.270102389799\,i$
$(10^4, 10^8)$	$1.0534774386626098 \times 10^7 + 10323.270102389799\,i$ $-1.053462615899727 \times 10^7 + 0\,i$ $148.22762883868868 + 10323.270102389799\,i$

Table 2. Checking for the IR-divergent cancellation of the decay rates $\Gamma_{\text{1-loop}}$ and Γ_{soft} at $k_C = 0.1$, $M_{WW} = 500$ GeV.

m_γ	$\Gamma_{\text{1-loop}}$	Γ_{soft}	$\Gamma_{\text{1-loop+soft}}$
10^{-10}	-8.81550898033887	8.963225158327703	0.1477161779888316
10^{-14}	-12.8788219949896	13.02653817297847	0.1477161779888316
10^{-18}	-16.9421350096404	17.08985118762925	0.1477161779888511

Table 3. Checking for the k_C-independent of the decay rates Γ_{soft} and Γ_{hard} at $M_{WW} =$ 500 GeV, photon mass m_γ is 10^{-10} GeV.

k_c	Γ_{soft}	Γ_{hard}	$\Gamma_{\text{soft+hard}}$
0.001	6.931568651002313	4.964814985732469	11.89638363673478
0.005	7.641602129869577	4.254791827098171	11.89639395696775
0.01	7.947396904665006	3.949009959152349	11.89640686381736

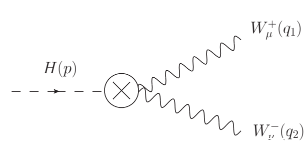

Fig. 6. Group 0: counter-term Feynman diagram.

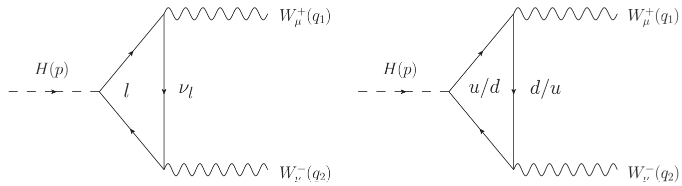

Fig. 7. Group 1: one-loop Feynman diagrams with exchanging doublet fermions in the loop.

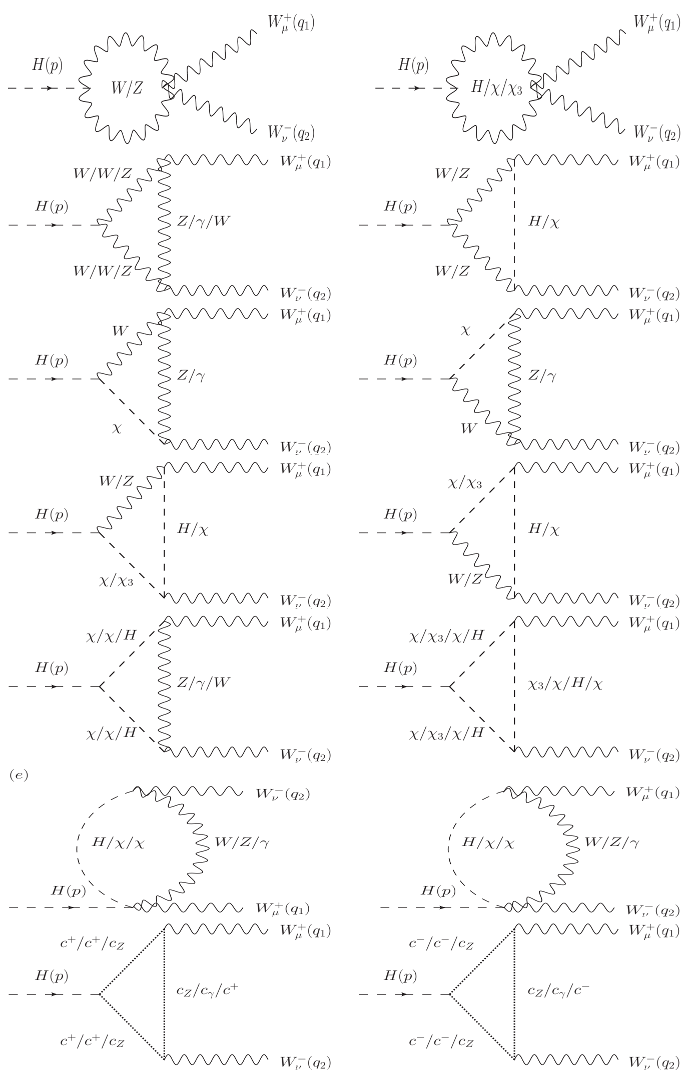

Fig. 8. Group 2: one-loop Feynman diagrams with exchanging boson and ghost particles in the loop.